Received: 26 September 2024 | Revised: 26 December 2024 | Accepted: 30 December 2024

DOI: 10.1002/cac2.12658

CANCER COMMUNICATIONS Open Access

LETTER TO THE JOURNAL

Single-cell multi-omics reveals tumor microenvironment factors underlying poor immunotherapy responses in ALK-positive lung cancer

Lung cancer remains the leading cause of cancer death in 2024, with ~80% being non-small cell lung cancer (NSCLC). Anaplastic lymphoma kinase (ALK) rearrangements occur in ~5% of NSCLC cases, typically treated with ALK inhibitors, though resistance often develops [1]. Immunotherapy has been explored for advanced or resistant ALK-positive NSCLC, but immune checkpoint blockade (ICB) treatments have shown limited clinical benefits [1].

A comprehensive study of ALK-positive NSCLC tumor microenvironment (TME) is needed to understand immunotherapy limitations and improve treatment strategies. We generated and collected single-cell RNA sequencing (scRNA-seq) and single-cell Assay for Transposase Accessible Chromatin with high-throughput sequencing (scATAC-seq) datasets from lung adenocarcinoma (LUAD) patients with ALK rearrangements and wild type without major oncogenic drivers (WT) (Supplementary Table S1). By comparing TME, we aimed to identify features explaining poor immunotherapy responses (Figure 1A).

After batch corrections for each of the RNA and ATAC profiles, we identified epithelial, stromal, and immune cells (Supplementary Figure S1A, Supplementary Table S2). From the immune compartment, we identified major cell types such as myeloid cells, T cells, natural killer (NK) cells, and B cells (Figure 1B, Supplementary Figure S1B, Supplementary Table S3). Integration of the RNA and ATAC profiles confirmed consistency between these two omics profiles (Supplementary Figure S1C-D). Compositional analysis revealed that ALK-positive samples showed an enrichment of innate immune cells (myeloid and NK cells) and depletion of adaptive immune cells (T and B cells) (Figure 1C, Supplementary Figure S1E-F), suggesting weak adaptive anti-tumoral responses in ALK-positive TME.

Oncogenic mutations primarily impact epithelial cells, so we classified epithelial cell malignancy with the cell-classifier and copy number variations (Supplementary Figure S1G-H) and measured *ALK* and *PD-L1* expression. Malignant cells expressing *ALK* or *PD-L1* were predominantly from ALK-positive malignant cells (Supplementary Figure S1I). We observed that ALK-positive tumors had a higher malignant-to-normal epithelial cell ratio than WT tumors (Figure 1D). Additionally, malignant cells in ALK-positive tumors exhibited increased stemness, indicating greater developmental potential (Figure 1E). Top 100 upregulated genes in ALK-positive tumors were linked to aggressive cancer pathways like epithelial-mesenchymal transition (EMT) and hypoxia [2] (Figure 1F).

To identify malignant subsets with higher progression potential, we constructed developmental trajectories (Supplementary Figure S1J). State 4, enriched with ALK-positive malignant cells, showed higher stemness and elevated stress, hypoxia, and EMT gene signatures (Supplementary Figure S1J-L, Supplementary Table S4). Survival analysis with LUAD patients in The Cancer Genome Atlas (TCGA) [3] showed worse outcomes for patients with higher expression of State 4 signature genes, while differentially expressed genes (DEGs) between ALK-positive and WT malignant cells did not predict survival (Supplementary Figure S1M). This suggested that ALK rearrangement leads to more aggressive and metastatic tumors and emergence of clinically unfavorable malignant sub-states.

Cell-cell interaction analysis showed ALK-positive malignant cells had increased interactions with myeloid cells (Figure 1G). Among these myeloid cell subtypes,

Abbreviations: NSCLC, non-small cell lung cancer; ALK, Anaplastic lymphoma kinase; ICB, Immune checkpoint blockade; TME, Tumor microenvironment; scRNA-seq, Single-cell RNA sequencing; scATAC-seq, Single-cell Assay for Transposase Accessible Chromatin with high-throughput sequencing; LUAD, Lung adenocarcinoma; WT, Wild type; NK, Natural killer; EMT, Epithelial-mesenchymal transition; TCGA, The Cancer Genome Atlas; DEG, Differentially expressed gene; TAM, Tumor-associated macrophage; TLS, Tertiary lymphoid structure; TCR, T cell receptor; TF, Transcription factor.

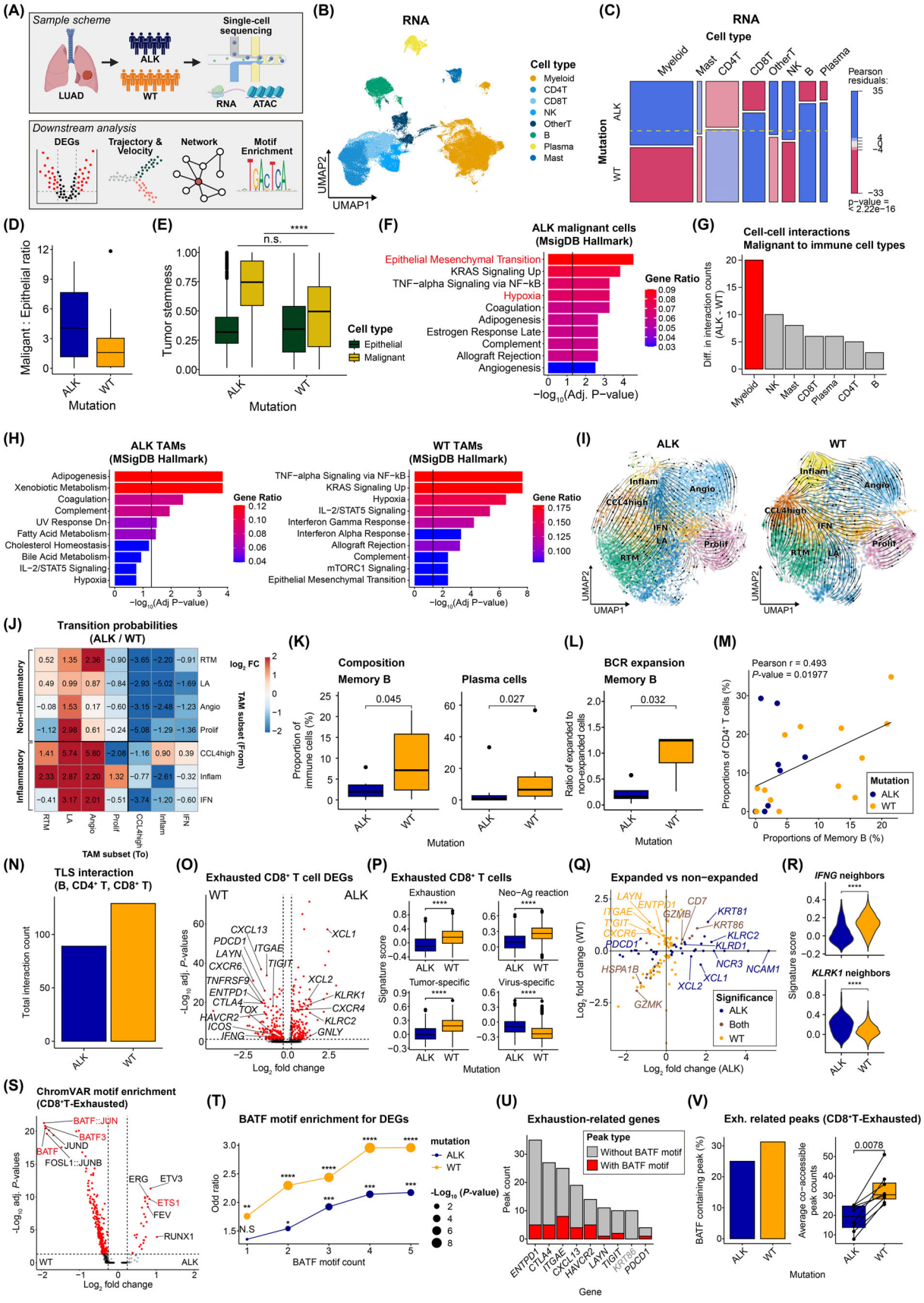

FIGURE 1 **Comparative analysis of TME of ALK-positive and WT lung cancer.** (A) Study scheme for single cell multi-omics data and downstream analysis. **(B)** UMAP plots of immune cells with batch-corrected scRNA-seq profiles, color-coded for cell types. We performed pre-processing, dimension reductions with batch correction, and clustering to obtain immune clusters. We annotated each cluster with

ALK-positive tumors had significantly higher proportions of tumor-associated macrophages (TAMs) (Supplementary Figure S2A). ALK-positive TAMs were linked to M2-like pro-tumoral functions like adipogenesis and lipid metabolism, while WT TAMs were associated with M1-like immune-related functions, including TNF-alpha signaling and interferon gamma response (Figure 1H). Sub-clustering of TAMs (Supplementary Figure S2B-C) and RNA velocity analysis revealed WT TAMs transitioned into anti-tumoral, inflammation-related states, whereas ALK-positive TAMs transitioned into pro-tumoral, metabolic states (Figure 1I-J, Supplementary Figure S2D),

corresponding cell types with cell type markers. **(C)** Mosaic plots for comparison of immune cell compositions between WT and ALK-positive groups for each omics approach. The color indicates Pearson residuals, showing enrichment or depletion of the cell types for each group. The yellow dashed lines represent the expected cell proportions, calculated by dividing the total cell counts for each mutation group by the overall total cell counts. Significance was calculated using the Chi-square test. **(D)** Ratio of malignant to normal epithelial cells for each mutation group. The malignant and normal epithelial cells were identified through the cell-classifier and detection of copy number variations. **(E)** Difference of tumor stemness scores between epithelial cell types for each mutation group. Transcriptome-based differentiation potential – indicating stemness for tumor cells – for each cell was calculated based on varieties of expressed genes and correlation patterns of commonly expressed genes for stem-like cells. Significance was calculated using two-sided Wilcoxon rank-sum test. n.s., not significant, ****$P < 0.0001$. **(F)** Pathway enrichment of top 100 upregulated genes in ALK-positive malignant cells compared to WT malignant cells for MsigDB Hallmark (2020) gene sets. The color indicates fractions of the query genes that overlap with each reference gene set. Significance was calculated using Fisher's exact test with the Benjamini-Hochberg correction. **(G)** Differences in the number of cell-cell interactions from each immune cell type to malignant cells between ALK-positive and WT samples. The cell-cell interactions between two cell types were calculated based on the expressions of known interacting ligands and receptors. **(H)** Pathway enrichment of top 50 upregulated genes in TAMs of ALK-positive tumors (left) and those of WT samples (right) for MsigDB Hallmark (2020) gene sets. The color indicates fractions of query genes that overlap with genes of each reference gene set. The *P*-values were calculated using the Fisher's exact test with the Benjamini-Hochberg correction. **(I)** Stream plots depicting cell transitions according to their RNA velocity for TAMs in ALK-positive tumors (left) and WT tumors (right). The RNA velocities were calculated by quantifying spliced and unspliced reads for each gene using Velocyto and modeling gene splicing kinetics with scVelo. **(J)** Heatmap depicting cell type transitions from row to column. The color indicates $\log_2$ fold changes calculated by dividing transition probability for TAMs in ALK-positive tumors by TAMs in WT tumors. **(K)** Proportions of memory B cells and plasma cells in tumor for each mutation group. Significance of the difference was calculated using the two-sided Wilcoxon rank-sum test. **(L)** Ratios of expanded to non-expanded memory B cells for each mutation group. Higher ratios indicate higher B cell activation and immune responses. B cells with BCR sequences that had two or more overlapping clones were defined as expanded cells. Significance of the difference was calculated using the two-sided Wilcoxon rank-sum test. **(M)** Scatter plot of relationship between proportion of memory B cells and proportion of $CD4^+$ T cells in each of mutation group. **(N)** Bar plots depicting total interactions among major components of tertiary lymphoid structure (TLS) composed of B cells, $CD8^+$ T cells, and $CD4^+$ T cells in ALK-positive and WT tumors. Cell-cell interaction counts among those cell types were added for each mutation group. **(O)** Volcano plot of DEGs of exhausted $CD8^+$ T cells between ALK-positive and WT tumors. The *P*-values were calculated using the two-sided Wilcoxon rank-sum test with Bonferroni correction. The significant genes are colored red. **(P)** Comparison of gene signature scores for gene sets related to functions and states of $CD8^+$ T cells for exhausted $CD8^+$ T cells between two mutation groups. Significance of the differences were calculated using the two-sided Wilcoxon rank-sum test. **(Q)** Visualization of two DEG analyses between expanded and non-expanded effector and exhausted $CD8^+$ T cells for each mutation group. T cells with TCR sequences that had five or more overlapping clones were defined as expanded cells. The genes are considered significant for each mutation group if the adjusted *P*-values < 0.05 (by two-sided Wilcoxon rank-sum tests with Bonferroni correction). **(R)** Gene signature scores for exhausted $CD8^+$ T cells with neighboring nodes to *IFNG* (top) and *KLRK1* (bot) within WT and ALK group, respectively. Cell-type specific networks were constructed for each cell types for each mutation group and neighboring nodes were defined as all connected nodes to the hub genes. The neighboring nodes to *IFNG* were defined in WT network whereas the neighboring nodes to *KLRK1* were defined in ALK network to generate gene signatures. **(S)** Volcano plot for differentially enriched chromVAR motifs for exhausted $CD8^+$ T cells. The peaks from scATAC-seq profiles were added with motif information and motif deviations compared to random peak sequences were calculated to generate motif deviation matrices. With those matrices, differentially enriched motifs were calculated. The *P*-values were calculated using the two-sided Wilcoxon rank-sum tests with Bonferroni correction. **(T)** Enrichment of genes with BATF motifs from DEGs of exhausted $CD8^+$ T cells between ALK-positive and WT groups. For each gene in the lists of DEGs, the number of BATF motifs was calculated and compared to genes not in the lists of DEGs. For each BATF motif count threshold, *P*-values and odd ratios were calculated using Fisher's exact tests for each mutation group. **(U)** Number of peaks related to exhaustion-related genes. Peaks were colored red for containing BATF motifs. **(V)** Characterization of peaks from exhausted $CD8^+$ T cells that are related to exhaustion genes. Percentages of peaks linked to the exhaustion genes that contained BATF motifs (Left). Average number of peaks co-accessible to peaks related to the exhaustion genes for each mutation group (Right). Peak co-accessibilities for each mutation group were calculated based on co-occurrences of those peaks for cells in each group. Abbreviations: LUAD, lung adenocarcinoma; ALK, Anaplastic lymphoma kinase; WT, wild type; scRNA-seq, single-cell RNA sequencing; scATAC-seq, Single-cell Assay for Transposase Accessible Chromatin with high-throughput sequencing; UMAP, uniform manifold approximation and projection; TAM, tumor-associated macrophage; Inflam, inflamed; Angio, angiogenesis; Prolif, proliferating; RTM, resident tissue-like macrophage; IFN, interferon; LA, lipid-associated; BCR, B cell receptor; TLS, tertiary lymphoid structure; DEG, differentially expressed gene; Exh., exhausted.

maintaining immunosuppressive TME in ALK-positive tumors.

Depleted adaptive immunity in ALK-positive tumors suggested reduced anti-tumoral immune functions [4]. B cell analysis (Supplementary Figure S2E-F) revealed that memory B cells and plasma cells were more abundant in WT tumors (Figure 1K). Top DEGs of WT memory B cells were enriched in oxidative phosphorylation pathways, indicating functional activation and effector capabilities [5] (Supplementary Figure S2G). Reconstructed B cell receptor sequences showed a lower ratio of expanded to non-expanded memory B cells in ALK-positive tumors (Figure 1L), suggesting reduced humoral anti-tumoral responses and activation. B cells are key components of tertiary lymphoid structures (TLSs), vital for immunotherapy responses [6]. We found positive correlations between B cells and $CD4^+$ T cells, with WT tumors having more B cells (Figure 1M). ALK-positive tumors showed reduced interactions among major components of TLS, suggesting fewer TLS-like structures (Figure 1N), contributing to inadequate anti-tumoral responses and unfavorable TME for immunotherapy. Further experimental validations would be beneficial to confirm the existence of TLS-like structures.

For $CD8^+$ T cells, crucial in ICB treatment, we identified subtypes using marker genes (Supplementary Figure S2H-I). DEG analysis showed tumor-reactive and exhaustion genes (*CXCL13, ENTPD1, ITGAE*) were enriched in WT tumors, while bystander-indicating NK receptors (*KLRK1, KLRC2*) [7] were enriched in ALK-positive tumors (Figure 1O). T cell signature analysis confirmed these findings (Figure 1P, Supplementary Table S4). This suggested that ALK-positive "exhausted" $CD8^+$ T cells became dysfunctional through non-canonical mechanisms, reducing their effectiveness during ICB treatment.

Single-cell T cell receptor (TCR) sequencing showed fewer expanded ALK-positive $CD8^+$ T cells with smaller TCR clonal sizes (Supplementary Figure S2J-K), indicating reduced T cell antigenicity. DEG analysis between expanded and non-expanded effector and exhausted $CD8^+$ T cells revealed WT tumors had increased expression of exhaustion and tumor-reactivity genes, while the ALK-positive tumors showed decreased expression of these genes and increased NK receptor expression (Figure 1Q). This reaffirmed impaired tumor reactivity and more bystander-like $CD8^+$ T cells in ALK-positive tumors.

We analyzed gene regulatory changes in exhausted $CD8^+$ T cell networks due to ALK rearrangement (Supplementary Figure S2L-M). In the WT network, T cell activation and exhaustion-related genes emerged as hubs with *IFNG* as a top hub gene, consistent with its role in effector T cell stimulation and reported deficiency in ALK-positive patients [1] (Supplementary Figure S2N). NK receptors like *KLRK1* had high centrality in the ALK-positive network. We re-evaluated hub genes based on neighboring gene expression signatures. *IFNG* signature score was higher in exhausted T cells of WT tumors, while *KLRK1* signature score was higher in exhausted T cells of ALK-positive tumors (Figure 1R).

Since T cell exhaustion is also epigenetically regulated, we identified $CD8^+$ T cell subtypes using scATAC-seq profiles and marker gene scores (Supplementary Figure S2O-P). Although transcription of exhaustion and tumor-reactivity genes was downregulated in ALK-positive $CD8^+$ T cells, no clear depletion in chromatin accessibility was observed (Supplementary Figure S2Q), suggesting transcription factor (TF) binding caused these differences. Motif analysis showed BATF-related TFs, linked to $CD8^+$ T cell effector functions [8, 9], were enriched in WT, while ETS1, important for NK cell differentiation [10], was enriched in ALK-positive cells (Figure 1S).

We hypothesized that BATF is a key TF contributing to differences in T cell dysfunction. Using DEGs in $CD8^+$ T cells between WT and ALK-positive tumors (see Figure 1O), we found WT DEGs had stronger BATF motif enrichment (Figure 1T) and all exhaustion/tumor-reactivity genes, except *KRT86*, had at least one peak with BATF motifs (Figure 1U). Interestingly, *KRT86*, the only exhaustion-related gene upregulated in expanded cells from both groups (see Figure 1Q), lacked BATF motifs. These findings suggested that differences in TF activities could lead to differences in gene expression. Additionally, WT exhausted T cells had more nearby peaks containing BATF motifs with higher co-accessibility, suggesting stronger co-regulation with nearby genomic regions in WT compared to the ALK-positive tumors (Figure 1V).

In summary, this study provides key insights into the TME of ALK-positive lung cancer through single-cell multi-omics analysis, shedding light on poor immunotherapy responses. ALK-positive tumors displayed aggressive malignant phenotypes, enriched pro-tumoral myeloid cells, and depleted adaptive T and B cells. ALK-positive TAMs shifted away from inflammatory states, while $CD8^+$ T cells showed reduced tumor reactivity and more bystander traits. We suggest that these $CD8^+$ T cells may have distinct dysfunction mechanisms. Epigenetic analysis revealed depleted BATF motifs in ALK-positive $CD8^+$ T cells, indicating altered TF activity. These findings highlight how ALK rearrangements drive an immunosuppressive TME, hindering effective immune responses, and suggest a need for strategies to reinvigorate adaptive immunity in ALK-positive lung cancer.

AUTHOR CONTRIBUTIONS

Hye Ryun Kim, Seong Yong Park, and Insuk Lee conceived the study. Seungbyn Baek performed single-cell multi-

omics data analysis under the supervision of Insuk Lee. Euijeong Sung assisted bioinformatic analysis. Gamin Kim contributed sample preparation. Hye Ryun Kim and Seong Yong Park organized clinical sample and data collections. Min Hee Hong and Chang Young Lee contributed to clinical sample collection. Hyo Sup Shim contributed to the pathological examination of tumor tissues. Insuk Lee and Hye Ryun Kim contributed to the financial and administrative support for this study. Seungbyn Baek, Hye Ryun Kim, and Insuk Lee wrote the manuscript. All authors read and approved the final manuscript.

ACKNOWLEDGEMENTS

Not applicable.

CONFLICT OF INTEREST STATEMENT

The authors declare that they have no conflicts of interest.

FUNDING INFORMATION

This research was supported by the Bio & Medical Technology Development Program of the National Research Foundation funded by the Ministry of Science and ICT (2021R1A2C2094629 and 2017M3A9E9072669 to Hye Ryun Kim, and 2018R1A5A2025079, 2022M3A9F3016364, and 2022R1A2C1092062 to Insuk Lee). The work was supported in part by Brain Korea 21 (BK21) FOUR program. This work was supported by the Technology Innovation Program (20022947) funded by the Ministry of Trade Industry & Energy (MOTIE, Korea). This work was supported by the Yonsei Fellow Program, funded by Lee Youn Jae.

DATA AVAILABILITY STATEMENT

The single-cell RNA, TCR, and ATAC sequencing data generated in this study are deposited in the Gene Expression Omnibus database with accession number GSE274934 (https://www.ncbi.nlm.nih.gov/geo/query/acc.cgi?&acc=GSE274934). The data will be available upon publication. The remaining data are available within the Article or Supplementary Information.

ETHICS STATEMENT

The studies were approved by the Institutional Review Board of Yonsei University Severance Hospital with IRB No 4-2018-1161-1. Written informed consent was obtained prior to enrollment and sample collection at Yonsei University Severance Hospital. The research conformed to the principles of the Helsinki Declaration.

Seungbyn Baek[1]
Euijeong Sung[1]
Gamin Kim[2]
Min Hee Hong[2]
Chang Young Lee[3]
Hyo Sup Shim[4]
Seong Yong Park[5]
Hye Ryun Kim[2]
Insuk Lee[1,6]

[1]*Department of Biotechnology, College of Life Science and Biotechnology, Yonsei University, Seoul, Republic of Korea*
[2]*Division of Medical Oncology, Department of Internal Medicine, Yonsei Cancer Center, Yonsei University College of Medicine, Seoul, Republic of Korea*
[3]*Department of Thoracic and Cardiovascular Surgery, Yonsei University College of Medicine, Seoul, Republic of Korea*
[4]*Department of Pathology, Yonsei University College of Medicine, Seoul, Republic of Korea*
[5]*Department of Thoracic and Cardiovascular Surgery, Samsung Medical Center, Sungkyunkwan University School of Medicine, Seoul, Republic of Korea*
[6]*Biotech Center, Pohang University of Science and Technology, Pohang, Republic of Korea*

Correspondence
Insuk Lee, Department of Biotechnology, College of Life Science and Biotechnology, Yonsei University, Seoul 03722, Republic of Korea.
Email: insuklee@yonsei.ac.kr

Hye Ryun Kim; Division of Medical Oncology, Department of Internal Medicine, Yonsei Cancer Center, Yonsei University College of Medicine, Seoul 03722, Republic of Korea.
Email: nobelg@yuhs.ac

Seong Yong Park; Department of Thoracic and Cardiovascular Surgery, Samsung Medical Center, Sungkyunkwan University School of Medicine, Seoul 06351, Republic of Korea.
Email: syparkcs@gmail.com

ORCID

Insuk Lee https://orcid.org/0000-0003-3146-6180

REFERENCES

1. Schenk EL. Narrative review: immunotherapy in anaplastic lymphoma kinase (ALK)+ lung cancer—current status and future directions. Transl Lung Cancer Res. 2023;12(2):322.
2. Fares J, Fares MY, Khachfe HH, Salhab HA, Fares Y. Molecular principles of metastasis: a hallmark of cancer revisited. Signal Transduct Target Ther. 2020;5(1):28.
3. Network CGAR. Comprehensive molecular profiling of lung adenocarcinoma. Nature. 2014;511(7511):543.
4. Chang RB, Beatty GL. The interplay between innate and adaptive immunity in cancer shapes the productivity of cancer immunosurveillance. J Leukoc Biol. 2020;108(1):363-376.

5. Waters LR, Ahsan FM, Wolf DM, Shirihai O, Teitell MA. Initial B cell activation induces metabolic reprogramming and mitochondrial remodeling. iScience. 2018;5:99-109.
6. Helmink BA, Reddy SM, Gao J, Zhang S, Basar R, Thakur R, et al. B cells and tertiary lymphoid structures promote immunotherapy response. Nature. 2020;577(7791):549-555.
7. Kim T-S, Shin E-C. The activation of bystander CD8+ T cells and their roles in viral infection. Exp Mol Med. 2019;51(12):1-9.
8. Kurachi M, Barnitz RA, Yosef N, Odorizzi PM, DiIorio MA, Lemieux ME, et al. The transcription factor BATF operates as an essential differentiation checkpoint in early effector CD8+ T cells. Nat Immunol. 2014;15(4):373-383.
9. Seo H, González-Avalos E, Zhang W, Ramchandani P, Yang C, Lio C-WJ, et al. BATF and IRF4 cooperate to counter exhaustion in tumor-infiltrating CAR T cells. Nat Immunol. 2021;22(8):983-995.
10. Taveirne S, Wahlen S, Van Loocke W, Kiekens L, Persyn E, Van Ammel E, et al. The transcription factor ETS1 is an important regulator of human NK cell development and terminal differentiation. Blood. 2020;136(3):288-298.

SUPPORTING INFORMATION

Additional supporting information can be found online in the Supporting Information section at the end of this article.